3414–3423 *Nucleic Acids Research, 2013, Vol. 41, No. 5* *Published online 11 January 2013*
doi:10.1093/nar/gks1468

Mycobacterium tuberculosis RsdA provides a conformational rationale for selective regulation of σ-factor activity by proteolysis

Ravi K. Jaiswal, Tangirala Surya Prabha, Gowravaram Manjeera and Balasubramanian Gopal*

Molecular Biophysics Unit, Indian Institute of Science, Bangalore 560 012, India

Received April 12, 2012; Revised December 9, 2012; Accepted December 17, 2012

ABSTRACT

The relative levels of different σ factors dictate the expression profile of a bacterium. Extracytoplasmic function σ factors synchronize the transcriptional profile with environmental conditions. The cellular concentration of free extracytoplasmic function σ factors is regulated by the localization of this protein in a σ/anti-σ complex. Anti-σ factors are multi-domain proteins with a receptor to sense environmental stimuli and a conserved anti-σ domain (ASD) that binds a σ factor. Here we describe the structure of *Mycobacterium tuberculosis* anti-σ^D (RsdA) in complex with the -35 promoter binding domain of σ^D ($\sigma^D{}_4$). We note distinct conformational features that enable the release of σ^D by the selective proteolysis of the ASD in RsdA. The structural and biochemical features of the σ^D/RsdA complex provide a basis to reconcile diverse regulatory mechanisms that govern σ/anti-σ interactions despite high overall structural similarity. Multiple regulatory mechanisms embedded in an ASD scaffold thus provide an elegant route to rapidly re-engineer the expression profile of a bacterium in response to an environmental stimulus.

INTRODUCTION

The ability of *Mycobacterium tuberculosis* to persist in the host for extended periods of time suggests an efficient intracellular response to environmental stimuli. A class of transcription factors, the extracytoplasmic function σ factors (ECF), exclusively synchronize changes in the transcription profile with environmental conditions. *M. tuberculosis* has 13 σ factors of which 10 belong to the ECF family. These σ factors play an important role in the complex life cycle of *M. tuberculosis* (1,2). A majority of ECF σ factors are localized in an inactive complex by their association with anti-σ factors. The anti-σ factor could either be cytosolic (for example, RsbW and Rv1222 in *M. tuberculosis*) or membrane associated (*M. tuberculosis* RsdA, RskA and RslA). The cellular concentration of free ECF σ factors is regulated by the release of this protein from an inhibited σ/anti-σ factor complex.

Multiple mechanistic routes have been demonstrated to regulate the release of a σ factor from a σ/anti-σ factor complex. The regulation of σ factor activity by a proteolytic cascade is best examined in the case of the *Escherichia coli* ECF, σ^E. RseA, the anti-σ factor for σ^E, is a receptor protein. RseA is proteolyzed by a two-step mechanism, and the proteolytic action of DegS triggers the activity of a membrane-embedded protease RseP. This results in the release of the cytosolic segment of RseA bound to σ^E. The anti-σ domain (ASD) of RseA is subsequently degraded by the ClpX–ClpP proteolytic complex. Caseinolytic protease (Clp) proteases degrade aggregated and denatured proteins or nascent proteins formed due to stalled ribosomes (3,4). Of the two components in the proteolytic complex, the protease subunit (ClpP) forms a pore-like structure that helps in the cleavage of the unfolded polypeptide. Two heptameric rings of ClpP interact with one hexameric ring of either ClpX or ClpA (5). The motor proteases (ClpX or ClpA) interact at either one or both ends of the ClpP pore. This assembly forms a hollow cylinder containing protease subunits capped at both ends by motor subunits that interact with the heptameric ring of ClpP (6). This arrangement (ClpX–ClpP or ClpA–ClpP complex) is similar to the eukaryotic proteasome, which has a central proteolytic cavity capped at both ends by ATPases (7). The choreographed action of membrane and cytosolic proteases is brought about by the exposure of a sequence motif in the ASD, and in this case, a 'VAA' motif at the C-terminus of cytosolic RseA (8,9). This regulatory mechanism has also been demonstrated for the *Bacillus subtilis* σ^W/RsiW and the *Pseudomonas aeruginosa* AlgU/MucA complexes (10–12). The existence

*To whom correspondence should be addressed. Tel: +91 80 2293 3219; Fax: +91 80 2360 0535; Email: bgopal@mbu.iisc.ernet.in or mbubgopal@gmail.com

of a similar proteolytic cascade in *M. tuberculosis* was demonstrated recently (13,14). *M. tuberculosis* Rip1 was identified as a site-2 protease for three membrane-associated anti-σ factors RskA, RslA and RsmA. *M. tuberculosis* RsdA was not affected by Rip1 activity (15). Conformational change triggered by environmental stimuli can also result in the release of a σ factor from a σ/anti-σ factor complex. In the case of *M. tuberculosis* σ^L/RslA, for example, conformational change on Zn^{2+} release governs the dissociation of the σ^L/RslA complex (16).

M. tuberculosis has only one ribosomal RNA operon—efficient transcription of this operon is thus a prerequisite for the survival of the bacillus. The σ^D regulates the expression of the ribosomal RNA operon. The σ^D deletion mutant (*M. tuberculosis* Δ*sigD*) was found to have lower expression levels of genes encoding constituents of the ribosome, elongation factors, DNA-binding proteins and enzymes involved in adenosine triphosphate (ATP) biosynthesis (17). Although the Δ*sigD* mutant showed persistence and colony-forming units similar to the wild type strain of *M. tuberculosis*, the time to death was significantly delayed (2,17). These studies suggested that σ^D maintains homeostasis in the late stationary phase of *M. tuberculosis* growth. Furthermore, similar to the *rel* deletion mutant in *M. tuberculosis,* it was noted that the so-called PE-PGRS proteins are up-regulated in the Δ*sigD* mutant. These proteins are recognized by the immune system (18). The expression level of *sigD* is up-regulated in response to starvation, down-regulated during macrophage infection and hypoxia while being relatively stable in the exponential phase and stationary growth conditions (2). The σ^D is also involved in the regulation of the resuscitation-promoting factor, a protein that plays a crucial role in the renewal of bacterial growth after starvation or stationary phase (18).

Here we describe the crystal structure of the ASD of RsdA in complex with the -35 promoter element recognition domain of σ^D ($\sigma^D{}_4$). Sequence analysis suggested the presence of a C-terminal ClpX recognition motif in the trans-membrane region of two *M. tuberculosis* anti-σ factors RsdA and RslA. We note that while the *M. tuberculosis* ClpX–ClpP1–ClpP2 proteolytic complex could specifically degrade the ASD of RsdA, the ASD of RslA was resistant to proteolysis. This observation suggests that sequence features alone are insufficient to trigger the proteolytic degradation of an ASD. The influence of conformational variations in the ASD in selective proteolytic regulation was examined by Molecular Dynamics (MD) simulations. MD simulations allow atoms and molecules to interact at a fixed temperature for a period of time. These interactions, which follow the laws of classical mechanics, provide information on atomic motion that can potentially rationalize biological mechanisms. MD simulations suggest that RsdA is more flexible than RslA. It thus appears likely that despite having a recognition sequence for proteolytic degradation, the release of σ^L from the σ^L/RslA complex is regulated by conformational changes in RslA triggered by the release of a Zn^{2+} cofactor (16). The structurally conserved ASD thus appears to encode distinct regulatory mechanisms providing an elegant route to synchronize intracellular σ-factor levels with an environmental stimulus.

MATERIALS AND METHODS

Expression and purification of recombinant proteins

The details of the expression constructs used to obtain recombinant σ^D, RsdA (Rv3413c), ClpX, ClpP1 and ClpP2 are summarized in Supplementary Table S1. A single primer-based approach was used to obtain point variants of RsdA (19). σ^D/RsdA and $\sigma^D{}_4$/RsdA were purified by a co-expression and co-purification strategy. All the proteins used in the proteolysis assays as well as crystallization trials were purified using the same protocol unless otherwise mentioned. In each case, the plasmid encoding the gene of interest was transformed into *E. coli* BL21(DE3). Transformed colonies were grown in Luria broth with appropriate antibiotic markers till the cell density reached an $O.D._{600}$ of 0.5–0.6. Cells were induced with 0.3 mM Isopropyl β-D-1-thiogalactopyranoside, and post-induction, the temperature was reduced to 18°C for 12–13 h. Thereafter, these cells were harvested at 6000 rpm followed by re-suspension and sonication in lysis buffer (50 mM Tris–HCl, pH 7.5 and 300 mM NaCl). The lysate was centrifuged at 15 000 rpm and subsequently incubated with Ni^{2+}-Nickel-nitrilo triacetic acid (NTA) affinity beads (Sigma-Aldrich, Inc.) for 1 h at 4°C. The bound protein was eluted by a gradient of imidazole concentration (5 mM to 200 mm). Further purification was achieved by size exclusion chromatography on a Sephacryl Hiprep 16/60 S-200 column (Amersham Biosciences) in a buffer containing 50 mM Tris–HCl, pH 8.0, 300 mM NaCl and 2% glycerol. The molecular weights of purified proteins were verified by liquid chromatography–electrospray ionization mass spectrometry (Bruker Daltonics, Inc.).

Crystallization and structure determination

Crystallization trials for $\sigma^D{}_4$ and the $\sigma^D{}_4$/RsdA complex were performed using sparse matrix screens (Hampton Research) with conditions being examined by both hanging drop as well as under oil methods at room temperature. The crystallization drops contained 2 µl of protein (8 mg/ml) and 2 µl of the crystallization condition. Diffraction quality crystals of $\sigma^D{}_4$ were obtained in a condition containing 1.0–1.3 M ammonium sulfate, 0.1 M Tris–HCl, 5% 2-methyl-2, 4-pentanediol, 3% glycerol, pH 7.8 in 3–4 weeks. Diffraction quality crystals of $\sigma^D{}_4$/RsdA complex were obtained in a condition containing 1.0–1.5 M ammonium sulfate, 0.1 M 4-(2-hydroxyethyl)-1-piperazineethanesulfonic acid (HEPES), 15–20% polyethylene glycol (PEG) 4000, pH 7.4 within 3–4 days. Crystals were flash frozen in liquid nitrogen using 7% glycerol as cryo-protectant. Diffraction data were collected at 0.978Å at the BM-14 beam-line of the European Synchrotron Radiation Facility, Grenoble. The data were integrated and scaled using iMOSFLM and SCALA (20,21). The initial phases of $\sigma^D{}_4$ were obtained using Phenix (22) by the Single-wavelength Anomalous Diffraction (SAD) method. The structure of

the $\sigma^D{}_4$/RsdA complex was solved by Molecular Replacement–Single-wavelength Anomalous Diffraction (MR-SAD) using the $\sigma^D{}_4$ model. An initial model of the complex was obtained using the Autobuild module of Phenix. Subsequent model building and refinement was performed using COOT (23) and Phenix. The fit of the model to the electron density was evaluated by COOT. It was important to use translation–libration–screw (TLS) restraints obtained from the TLSMD server (24) to achieve convergence in refinement.

Molecular dynamics simulations

MD simulations were performed using the GROMACS v4.0.2 package with OPLS-AA/L force field (25,26). During the simulations, crystallographic water molecules were removed and the protein model was solvated with the TIP4P water model. All simulations used the isothermal–isobaric ensemble (constant pressure of 1 bar and temperature set to 300 K). Energy minimizations were performed using the conjugate gradient and steepest descent methods with a frequency of the latter set to 1 in 1000. Simulations were performed with full periodic boundary conditions. Bonds were constrained with the LINear Constraint Solver (LINCS) algorithm (27). The $\sigma^D{}_4$, $\sigma^D{}_4$/RsdA complex, RsdA, $\sigma^L{}_4$/RslA complex and RslA structural models were subjected to MD simulations for 50 ns. Structure analysis was performed by GROMACS tools and local unix scripts. Graphical representations were prepared using the Sigma-plot software (Systat Software). Secondary structural elements were ascertained using the Dictionary of Secondary Structure of Proteins (DSSP) software (28). The protein–protein interaction interface was analyzed using the Contact program from the CCP4 suite, while the interaction networks were represented using cytoscape (21,29).

Protease assays

All protease assays were performed in a buffer containing 25 mM HEPES–KOH (pH 7.5), 5 mM KCl, 5 mM $MgCl_2$, 0.02% NP-40 and 10% glycerol at 37°C (8). To monitor the proteolysis of $RsdA^{1-94}$ and $RslA^{1-125}$, Clp proteases (ClpX: 0.3 μM, ClpP1, ClpP2 or ClpP1–ClpP2: 0.8 μM), ATP (4 mM) and an ATP-regeneration system (50 μg/ml creatine kinase and 2.5 mM creatine phosphate) were pre-incubated and anti-σ factor substrates [$RsdA^{1-94}$, σ^D/$RsdA^{1-94}$, σ^L/$RslA^{1-125}$or $RslA^{1-125}$ (5.0–6.0 μM)] were added. Samples were removed at different time intervals, and a western blot was performed using anti-histidine monoclonal antibodies (GE Healthcare) at 1:2000 dilution for the detection of RsdA and RslA, while the σ factors were probed with anti-σ^D and anti-σ^L monoclonal antibodies at 1:2000 dilution. Immunoblots were developed with 3-amino-9-ethylcarbazole (Sigma-Aldrich, Inc) and H_2O_2 for peroxidase-attached secondary antibodies.

Surface plasmon resonance measurements

Interaction between σ^D and RsdA and $\sigma^D{}_4$ and RsdA were examined using surface plasmon resonance (SPR) (BIACORE 3000; GE Healthcare). σ^D and $\sigma^D{}_4$ were immobilized on a CM5 chip (BIACORE; GE Healthcare) at a surface density of 12 ng/mm^2. RsdA and the W50A mutant of RsdA were used as analytes in this study. The interaction kinetics was evaluated using BIAevaluation software. The first lane of the chip was used as control and all the interactions were examined in a buffer containing 20 mM Tris–HCl and 300 mM NaCl (pH 7.8).

RESULTS AND DISCUSSION

Crystallization and structure determination of $\sigma^D{}_4$ and the $\sigma^D{}_4$/RsdA complex

RsdA is the cognate anti-σ factor for σ^D and full-length σ^D interacts with the cytosolic component of RsdA (30). Crystallization trials were performed to obtain crystals of full-length σ^D and the ASD of RsdA ($RsdA^{1-80}$). The crystalline precipitates from these experiments, however, could not be improved. Crystals appeared after a month; these corresponded to $\sigma^D{}_4{}^{141-212}$ and RsdA. A recombinant protein fragment based on this finding ($\sigma^D{}_4$ and RsdA co-expressed in *E. coli*) yielded crystals of the $\sigma^D{}_4$/RsdA complex within 2–3 days. In the subsequent description of this complex, the sequence lengths of $\sigma^D{}_4$ and RsdA correspond to the protein construct in the $\sigma^D{}_4$/RsdA complex structure; variations in the sequence length used for biochemical analysis are explicitly noted (Supplementary Table S1). The data collection, refinement and model statistics are presented in Table 1.

Structure of $\sigma^D{}_4$ in the free and RsdA-bound form

The $\sigma^D{}_4$ structure could be superposed on other σ_4 models with a root-mean-square deviation (r.m.s.d.) of 1.2 Å (Figure 1a; Supplementary Figures S1a and b). The $\sigma^D{}_4$ structures determined independently for the free form and the $\sigma^D{}_4$/RsdA complex are not substantially different (r.m.s.d. of 0.7 Å between C^α atoms). The structural similarity between the free and bound forms of $\sigma^D{}_4$ suggests that unlike the structure of the *E. coli* σ^A/AsiA complex (33) where domain 4 of σ^{70} adopts a different conformation in the anti-σ bound form, the $\sigma^D{}_4$ conformation is not altered on binding RsdA. The stoichiometry observed in the crystal structure of the $\sigma^D{}_4$/RsdA complex is consistent with solution studies, and both $\sigma^D{}_4$/RsdA and σ^D/RsdA complexes adopt a 1:1 interaction stoichiometry in solution.

There are four molecules of the $\sigma^D{}_4$/RsdA complex in the asymmetric unit. In each protomer, RsdA adopts an identical conformation with two helices connected by a loop. The C-terminal helix could not be modeled due to poor electron density. Helix H1 of RsdA interacts with helices H1' and H4' of $\sigma^D{}_4$, while helix H3 interacts with H4' of $\sigma^D{}_4$ (Supplementary Figure S1). The buried surface area in the $\sigma^D{}_4$/RsdA complex is 1067.5Å^2, comparable with other σ_4/ASD complexes (Supplementary Table S2). A superposition of the $\sigma^D{}_4$/RsdA complex on the *E. coli* σ^E promoter DNA complex structure suggests that σ^D is inactivated by the occlusion of -35 promoter element binding region. The interaction between σ_4 and the anti-σ factor could potentially also facilitate regulatory mechanisms involving other proteins or small

Table 1. Data, phasing and refinement statistics

Crystal	σ^{D}_4	σ^{D}_4/RsdA
PDB ID	3VFZ	3VEP
Wavelength (Å)	0.978	0.978
Resolution (Å)[a]	33.88–1.90 (2.0–1.9)	49.87–2.5 (2.64–2.50)
Unit cell parameters (Å)	a = 80.43, b = 35.70, c = 50.92 β = 122.59	a = 99.74, b = 110.72, c = 73.13 β = 133
Space group	C121	C121
Total number of reflections[a]	69 206 (10 166)	139 525 (22 123)
Number of unique reflections[a]	9711 (1422)	18 114 (2855)
Completeness (%)[a]	99.6 (99.6)	98.3 (97.9)
Multiplicity[a]	7.1 (7.1)	7.7 (7.7)
R_{merge} (%)[a,b]	6.2 (58.8)	6.8 (44.2)
$<I>/\sigma(I)$[a]	17.9 (3.4)	15.6 (4.4)
II. Phasing		
	Selenium (SAD)	Selenium (MR-SAD)
Figure of merit	0.38	0.36
III. Refinement statistics		
R_{cryst} (%)/R_{free} (%)[c]	19.8/23.8	24.3/28.7
RMS_{bond} (Å)	0.006	0.015
RMS_{angle} (degree)	0.900	1.832
B factor (Å^2)[d]	46.96	53.62

[a]Values in parentheses are for the highest-resolution shell.
[b]$R_{merge} = \sum \sum_I |I(h)|$, where I(h) is the mean intensity after rejections.
[c]$R_{cryst} = \sum | Fp\text{-}Fc| / \sum |Fp|$; R_{free}, the same as R_{cryst} but calculated on 5% of data excluded from refinement.
[d]Averaged over all atoms.

molecule effectors. These possibilities are best exemplified in the case of the *E. coli* σ^{70}_4/Rsd complex. *E. coli* σ^{70}_4 binds the β-flap tip of the RNA polymerase enzyme and is a target for transcriptional activators in addition to its role in -35 promoter element binding. Three exposed cavities on distinct surfaces of Rsd in the *E. coli* σ^{70}_4/Rsd complex could potentially rationalize small molecule effector binding (34–36). A common theme that emerges from these structures is that regulation of σ-factor activity by the anti-σ factor involves occlusion of interacting surfaces in σ_4 rather than conformational changes in the σ_4 domain.

The anti-sigma domain of RsdA

In all ASDs structurally characterized thus far, helices H1 and H3 are required for interaction with σ_4, while H2 helps in positioning helices H1 and H3 to interact with the σ factor. The fourth helix (H4) binds σ_2 (32). The first three helices were noted to be well conserved across all anti-σ–factor structures. In the σ^{D}_4/RsdA structure, the ASD has only two helices; helix H2 is a loop in RsdA, while H4 could not be modeled owing to poor electron density (Figure 1a).

Although RsdA had a loop instead of helix H2, the orientation of helices H1 and H3 is similar to other ASDs. This is seen from the structural superposition of helices H1, H2 and H3 of RslA (r.m.s.d. of 2.7 Å over 27 α-carbon positions), RseA (r.m.s.d. of 2.1 Å over 33 α-carbons) and ChrR (r.m.s.d. of 2.0 Å over 34 α-carbons) on RsdA (Figure 1d). Superposition of ASDs also suggests that helix H3 is the most conserved secondary structural element when compared with helices H1 and H2. A sequence search revealed other ASDs similar to RsdA. Protein sequences corresponding to genes that have an ECF σ factor in the same operon, share at least 30% identity and possess a trans-membrane segment were considered as putative anti-σ factors for this analysis. Sequence-based secondary structure prediction performed using PSIPRED (37) suggests three helices instead of four—a finding consistent with the crystal structure of RsdA (Figure 1c; Supplementary Figure S1c and Supplementary Table S3). Another interesting observation from the multiple sequence analysis (38) is that the cytosolic ASDs of these trans-membrane proteins are better conserved than their periplasmic domains.

The ASD is a common structural fold in ECF (also referred to as group IV) anti-σ factors. While the fold of the ASD is conserved, the interactions between an ASD and a cognate σ factor show substantial variations. This feature was noted from several characterized σ_4/ASD complexes. Thus while the conformation of σ_4 is distorted in both *E. coli* σ^{70}/AsiA and the *Rhodobacter sphaeroides* σ^{E}/ChrR complexes, this is not the case in either *E. coli* σ^{E}/RseA or the *M. tuberculosis* σ^{L}_4/RslA or σ^{D}_4/RsdA complex. A comparison between the ChrR and RseA ASDs suggested that while the secondary structural content and tertiary arrangement of helices 1–3 are conserved, sequence diversity leads to differences in σ_4 interactions. The *M. tuberculosis* σ^{D}_4 and the σ^{D}_4/RsdA structures reveal a new variant that the tertiary conformation is more conserved than the helical content in the ASD. A structural Zn^{2+} has also been suggested to maintain the tertiary conformation of an ASD leading to a mechanistic hypothesis that the release of the bound Zn^{2+} cofactor in oxidative conditions regulates σ/anti-σ factor interactions. This mechanism is different from a proteolysis mechanism first proposed in the case of *E. coli* RseA. In this case, selective exposure of sequence motifs precede a proteolytic cascade that eventually leads to the degradation of an anti-σ factor. In both these

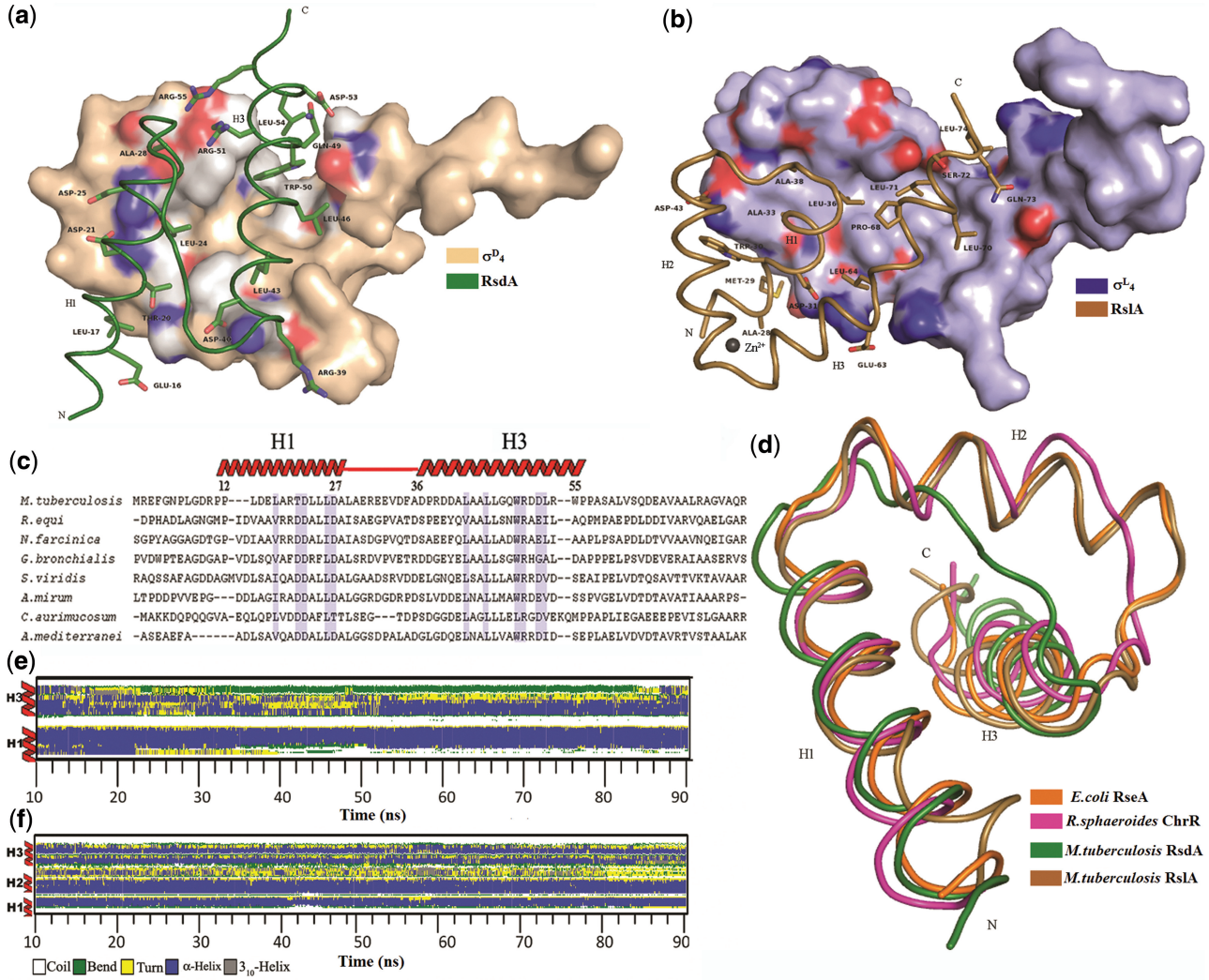

Figure 1. Structure of σ^{D}_4/RsdA complex. (**a**) In this representation, the C^{α} backbone of RsdA (green) is shown on the surface of σ^{D}_4 (wheat). The residues at the interface of σ^{D}_4 that interact with RsdA are highlighted. These interacting residues (based on a cut-off criterion of 4 Å) reveal that the σ^{D}_4/RsdA interface is substantially hydrophobic in nature. (**b**) Helix H2 of RslA is not involved in σ^{L}_4/RslA interactions. The C^{α} backbone trace of RslA (sand color) on the surface of σ^{L}_4 (blue) also shows the location of the Zn^{2+} cofactor vis-à-vis the σ^{L}_4/RslA interface. The residues at the σ^{L}_4/RslA interface are highlighted (16). (**c**) Sequence alignment of RsdA homologs reveals conserved residues that are buried at the σ^{D}_4/RsdA interface (gray background). The secondary structure annotations are based on the *M. tuberculosis* RsdA structure. (**d**) The ASDs of *M. tuberculosis* RsdA (green), *M. tuberculosis* RslA (sand) (16), *R. sphaeroides* ChrR (pink) (31) and *E. coli* RseA (orange) (32) are superposed over the first three α helices (H1–H3). (**e**) Time evolution of secondary structural elements in RsdA during the course of MD simulations. DSSP annotation was used to determine the secondary structural information. In this representation, the helical conformation is shown in blue, turn in yellow, bend in green and coil in white. The time-evolution profile reveals that the polypeptide stretch corresponding to H2 of the classical ASD fold remains disordered during the course of the MD simulations. (**f**) The secondary structural contents do not substantially vary in the time course of MD simulations on RslA. The secondary structure annotations are same as panel e.

mechanisms, conformational changes induced either temporally by environmental conditions or irreversibly due to proteolysis lead to the release of a free, active σ-factor. However, the sequence-structure determinants that dictate the choice of a regulatory mechanism remained unclear. A comparison between the σ^{L}_4/RslA and the σ^{D}_4/RsdA complexes provided an opportunity to examine these different regulatory mechanisms.

Conformational dynamics of the ASD

MD simulations were performed on the canonical ASD of *E. coli* RseA as well as the ASDs in *M. tuberculosis* RslA and RsdA. These simulations were performed to examine if the differences between the crystal structures of the ASDs in RsdA and RslA were functionally significant, i.e. the conformational features of these ASDs dictated the regulatory mechanisms adopted by these proteins. In all cases, the simulations stabilized within 10 ns (Supplementary Figure S2a and b). Clustering of the conformers was based on the α-carbon r.m.s.d. of simulated conformers at different time-points with respect to the crystal structure (39). The normalized population distribution obtained for the RsdA model in the free form (simulations on the RsdA model alone) and the bound form (simulations on the σ^{D}_4/RsdA complex) resulted in two major peaks in the bound form and three distinct conformational

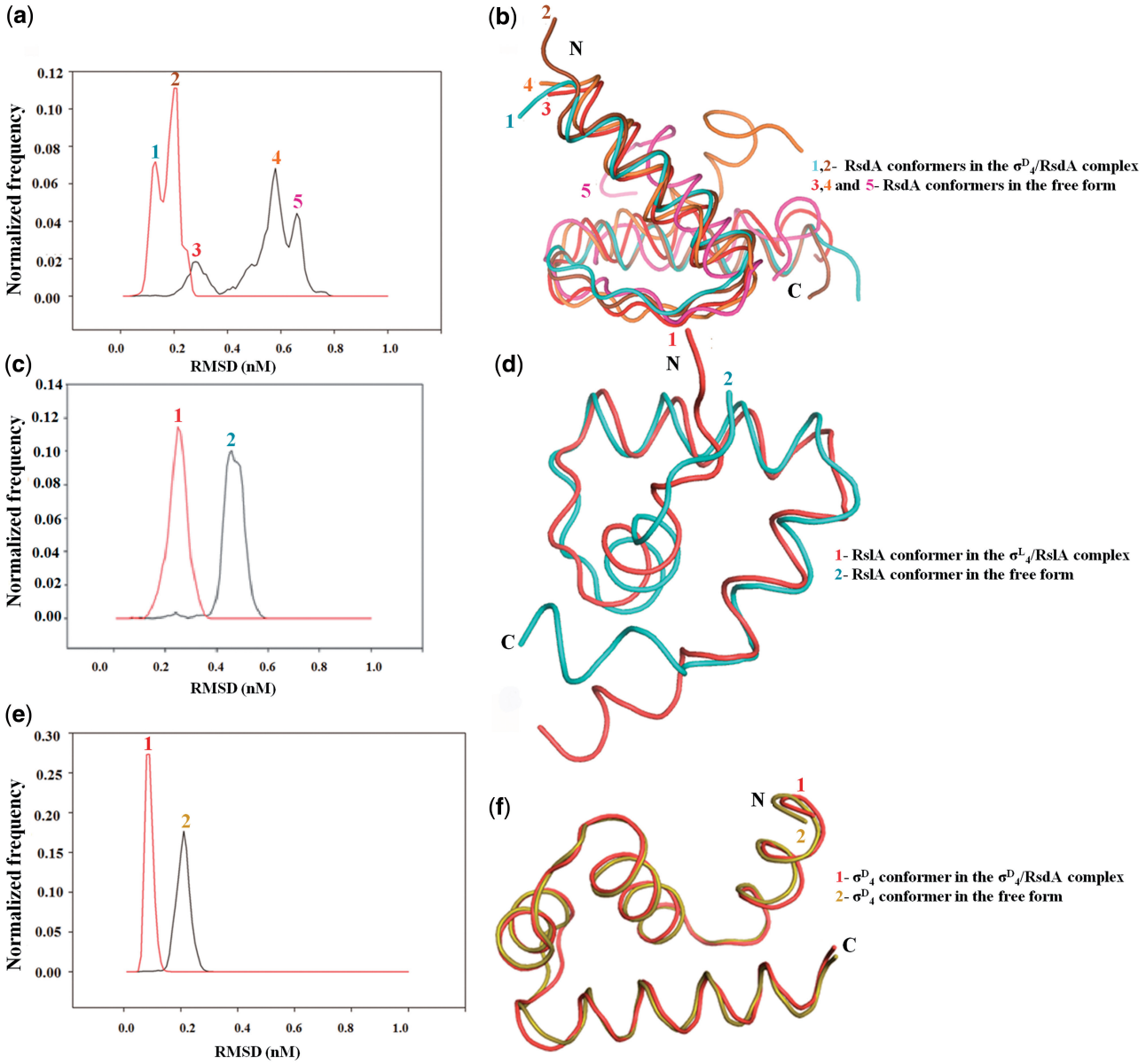

Figure 2. Conformational ensembles of the ASDs in RsdA and RslA. (**a**) MD simulations suggest that *M. tuberculosis* RsdA adopts different conformations in the σ^{D}_{4}/RsdA complex (red; peaks 1 and 2) and free form (black; peaks 3, 4 and 5). The r.m.s.d. values were determined with respect to the initial model (crystal structure) (**b**) Superposition of α-carbon atoms of representative structures from each peak. Structures corresponding to peak 1 (cyan), peak 2 (brown), peak 3 (red), peak 4 (orange) and peak 5 (pink) are shown. (**c**) Population distribution of RslA in the σ^{L}_{4}/RslA complex (red, peak 1) and the free form (black, peak 2). The r.m.s.d. are with respect to the crystal structure. (**d**) Superposition of the C^{α} traces corresponding to representative structures from each conformational ensemble. Structures representing peak 1 (red) and peak 2 (cyan) are shown. (**e**) The conformational ensembles derived from MD simulations on σ^{D}_{4} in the σ^{D}_{4}/RsdA complex (red; peak 1) and the free form (black; peak 2). (**f**) A superposition of the C^{α} traces corresponding to representative structures from peak 1 (red) and peak 2 (yellow) reveal minor conformational changes.

ensembles in the free form (Figure 2a). A superposition of the conformers illustrates the differences between free and bound forms of RsdA (Figure 2b). A comparison between these conformational ensembles revealed a change in the conformation of RsdA (r.m.s.d. of 5 Å over α-carbons) between the free and anti-σ–bound states. Helices H1 and H3 of RsdA undergo conformational changes accompanied by a helix to loop transition of helix H1. RsdA lacks helix H2. The simulations suggest that the loop in RsdA does not adopt an α helical conformation. Furthermore, no secondary structural transitions in H2 in either RseA or RslA were seen (Figure 1e and f). The results of these simulations are consistent with far ultraviolet circular dichroism (CD) spectra on these protein samples (Supplementary Figure S3). In these spectroscopic studies, α-helicity was induced by the addition of trifluoroethanol (40). The larger increase in the α-helical content of RsdA in the free form is consistent with the observation made on the basis of the crystal structure and MD simulations.

The difference in the radius of gyration of RsdA between the free form and the σ^{D}_{4}/RsdA complex suggest that RsdA in the free form is more compact

when compared with the bound form. This holds true even in the case of RslA (Supplementary Figure S2c). Simulations with the RslA structure and the σ^{L}_4/RslA complex suggested two prominent conformational ensembles—one associated with the free state, and one for the complex (Figure 2c). In this case, a structural superposition of the two conformers suggests that helix H3 of RslA changes conformation between free and the σ^{L}_4 bound states (Figure 2d). In this context, we note that no conformational changes were seen either between the crystal structures of free σ^{D}_4 or σ^{D}_4 in the σ^{D}_4/RsdA complex or the σ^{D}_4 conformation obtained from MD simulations (Figure 2e and f). Put together, these simulations suggest that conformational changes are localized to the ASD on binding the cognate σ factor.

Interactions between the ASD of RsdA and σ^{D}_4

The binding affinity of the RsdA ASD to σ^{D}_4 and full-length σ^{D} was determined by SPR experiments. Analysis of SPR sensograms suggest a dissociation constant (K_d) of *ca* 10 μM and 2 μM for σ^{D}_4 and full-length σ^{D}, respectively (Figure 3a and b) (Table 2). The binding affinity is less than that reported for the σ^{L}/RslA complex (20 nM) or the σ^{E}/RseA complex (10 pM) (8,16). We note that the buried surface area in the σ^{L}_4/RslA, σ^{E}_4/RseA and the σ^{D}_4/RsdA complexes are broadly similar (Supplementary Table S2). The differences in the binding affinity are thus likely due to differences in the sequence composition or the flexibility of the ASD. An observation from the multiple sequence alignment suggested Trp50 to be well conserved across RsdA homologs (Figure 1c). Additionally, MD simulations suggested Trp50 to be important in σ^{D}_4/RsdA interactions (Figure 3d). This observation was validated experimentally using a W50A mutant of RsdA. The W50A mutant showed a 10-fold reduction in binding affinity when compared with wild type RsdA (Figure 3c). MD simulations of the σ^{L}_4/RslA and the σ^{D}_4/RsdA complexes also reveal differences in the protein–protein interaction interface. A network of interface residues was identified based on their interactions during MD simulations of the σ^{D}_4/RsdA and σ^{L}_4/RslA complexes. Interface residues in the σ^{D}_4/RsdA complex were Leu24, Leu43, Leu46, Leu47 and Trp50. These residues make the most number of contacts with σ^{D}_4 during the course of simulation. Similarly, conserved

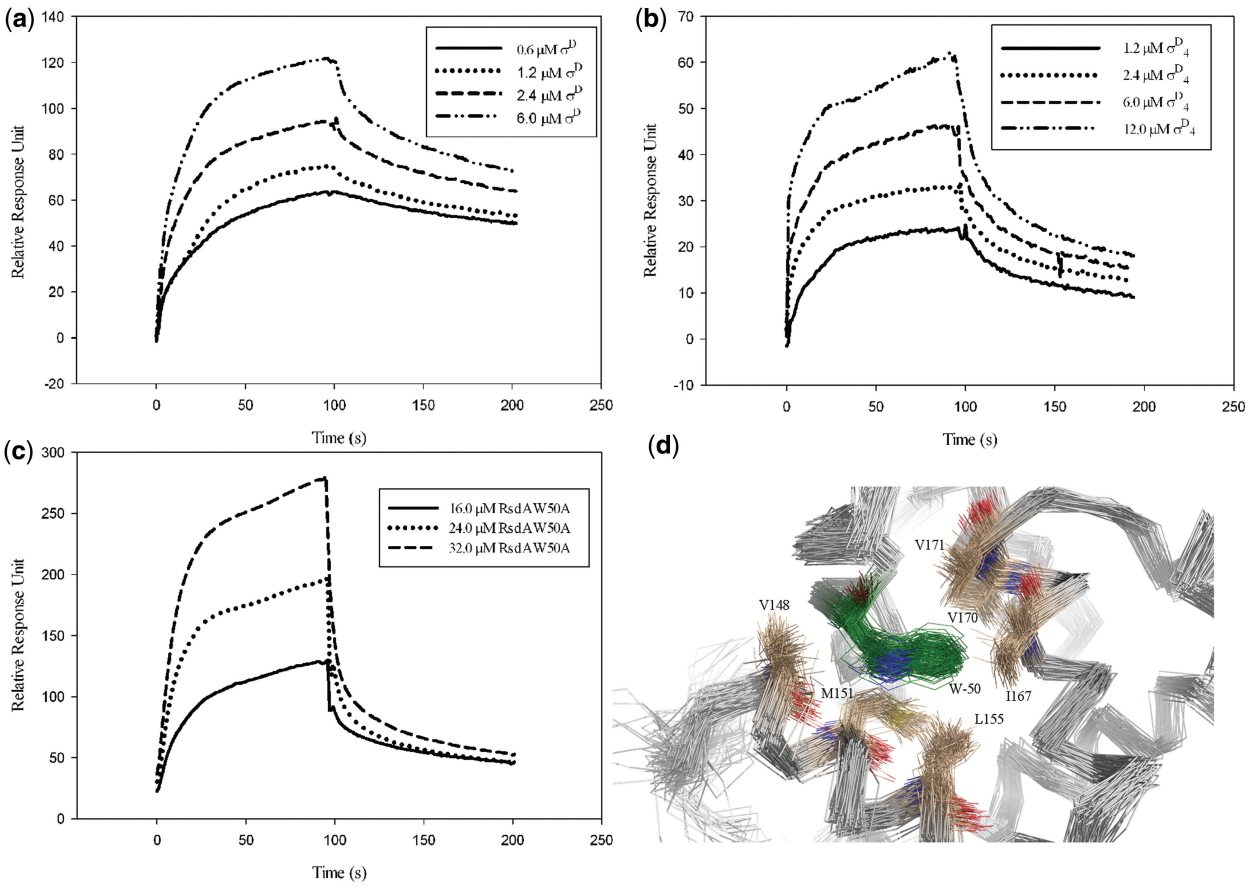

Figure 3. SPR sensograms for the interaction of σ^{D} with RsdA. (**a**) SPR measurements of σ^{D}/RsdA interactions reveal that the binding affinity of full-length σ^{D} (containing both σ^{D}_2 and σ^{D}_4 domains) with RsdA is *ca* 2.0 μM. (**b**) Interaction of σ^{D}_4 with RsdA reveals a 4-fold reduction in the binding affinity when compared with full-length σ^{D}. (**c**) The conserved tryptophan residue in RsdA (W50) contributes substantially to σ^{D}/RsdA interactions. The $RsdA^{1–94}$W50A point mutant interacts with σ^{D} with a 10-fold reduction in the binding affinity (corresponding to a K_d of 20μM). (**d**) MD simulations support the role of Trp50 in σ^{D}/RsdA interactions. A superposition of structures obtained during the course of MD simulations reveal that interactions between Trp50 of RsdA and residues of σ^{D}_4 (Val148, Met151, Leu155, Ile167, Val170 and Val171) are conserved during the course of MD simulations. In this representation, the α-carbon trace is shown in gray.

residues at the σ^{L}_4/RslA interface are Leu71, Leu74, Val67, Gln73 and Ala38. These residues are shown in the interaction network of σ^{D}_4/RsdA and the σ^{L}_4/RslA complexes (Supplementary Figure S4). An analysis of these interaction networks also suggests that the σ/anti-σ interface is largely hydrophobic. This observation is similar to that seen in the σ^{E}/RseA or the σ^{E}/ChrR σ/anti-σ complex.

RsdA is selectively degraded by the ClpX–ClpP proteasomal complex

Activation of the ECF σ factor σ^{E} by the selective proteolysis of the anti-σ factor RseA is well characterized in *E. coli*. DegS, a site-1 protease, and RseP, a site-2 protease, cleave RseA into periplasmic and intramembrane regions. The ASD of RseA is released into the cytosol with a 'VAA' sequence motif at the C-terminus (41). This is then selectively proteolyzed by Clp proteases (8). Neither site-1 nor site-2 proteases that act on *M. tuberculosis* RsdA have been identified thus far. However, sequence analysis revealed a similar sequence motif (VAA) to that of *E. coli* RseA (this motif is AAA in RslA) in the transmembrane region (Supplementary Figure S5). *M. tuberculosis* and *E. coli* ClpX and ClpP proteases share >50% sequence identity and the active site residues are well conserved (42). *M. tuberculosis* has two ClpP proteins, ClpP1 and ClpP2. A mixed ClpP1–ClpP2 complex was shown to be active against small peptides and proteins on binding N-blocked dipeptide activators (14). Experiments with freshly purified *M. tuberculosis* ClpX, ClpP1 and ClpP2 revealed that $RsdA^{1-94}$, both in the free form and in complex with σ^{D}, is proteolyzed specifically by the ClpX–ClpP1–ClpP2 proteasomal complex. We note that while the ClpX–ClpP1 proteasomal complex is inactive, proteolytic activity of ClpX–ClpP2 is substantially enhanced by the addition of ClpP1 (Figure 4a). This observation is similar to that of the anti-σ factor *M. tuberculosis* RseA, where the ClpC1–ClpP2 complex was able to cleave RseA specifically in a phosphorylation-dependent manner, whereas the ClpC1–ClpP1 assembly could not (43). These observations are consistent with the crystal structure of *M. tuberculosis* ClpP1 that revealed a smaller pore size compared with other ClpP

Table 2. Comparison of the binding affinity of characterized σ/anti-σ complexes

Construct	Dissociation constant (K_d)
σ^{D}/$RsdA^{1-94}$	2.6 ± 1.8 μM
σ^{D}_4/$RsdA^{1-94}$	10.3 ± 3.5 μM
σ^{D}/$RsdA^{1-94}$W50A	20.1 ± 4.2 μM
σ^{L}/$RslA^{1-108}$[a]	20.0 nM
σ^{E}/$RseA^{1-90}$[b]	10.0 pM

[a]Dissociation constants for *M. tuberculosis* σ^{L}/RslA obtained from (16).
[b]Data for *E. coli* σ^{E}/RseA noted from (8).

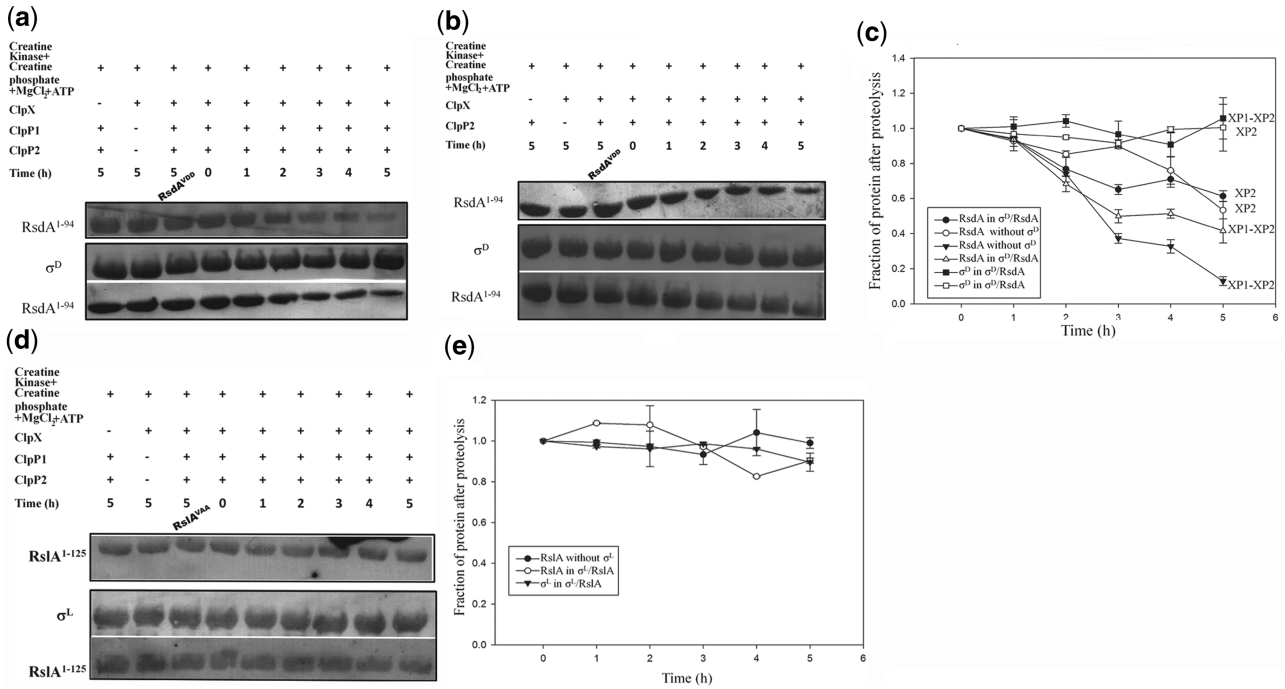

Figure 4. Activation of σ^{D} by the selective proteolysis of RsdA. (**a** and **b**) The ClpX–ClpP1–ClpP2 proteasomal assembly degrades RsdA, whereas RslA is resistant to proteolysis *in vitro*. These proteolysis experiments reveal that the proteolytic assembly is most efficient in the case of a ternary complex that contains ClpX, ClpP1 and ClpP2. Samples were obtained at specific time intervals. Immunoblots were performed using anti-histidine monoclonal antibodies (for RsdA and RslA), whereas σ^{D} and σ^{L} were detected by antibodies raised against purified recombinant σ^{D} and σ^{L}. The relative influence of the sequence motifs was examined by mutational analysis (VAA to VDD in RsdA; AAA to VAA in RslA). These are shown in lane 3 of the immunoblots. (**c**) A quantitative representation of the data shown in panels (a and b). Each data point corresponding to the fraction of protein retained after proteolysis represents an average of three experiments. (**d** and **e**) The ClpX–ClpP1–ClpP2 assembly does not affect the σ^{L}/RslA complex. Mutation of the recognition motif AAA to VAA does not convert RslA into a proteolytically labile ASD. These results are quantified in panel (e).

assemblies potentially making this protease subunit inactive (13,44,45). The proteolytic mechanism that governs the dissociation of the *M. tuberculosis* σ^D/RsdA complex is thus similar to the *E. coli* σ^E/RseA system. It was also demonstrated that the *E. coli* $RseA^{1-108}$ VDD mutant was resistant to proteolysis by Clp proteases (41,46). The VAA motif at the C-terminus of $RsdA^{1-94}$ was mutated to VDD. A truncated version of the RsdA ASD that lacks the 'VAA' sequence motif was also examined (data not shown). The VDD as well as the truncated mutants of RsdA were resistant to proteolysis by the ClpX–ClpP1–ClpP2 complex (Figure 4a). Surprisingly, $RslA^{1-125}$AAA both in the free state as well as in complex with σ^L was resistant to degradation either by the ClpX–ClpP1 or ClpX–ClpP2 or the ClpX–ClpP1–ClpP2 protease assemblies, either in the apo (Zn^{2+}-free) form or the holo (Zn^{2+}-bound) forms (Figure 4e). Addition of the sequence motif to RslA (mutating the AAA motif to VAA) did not appear to induce proteolytic susceptibility in RslA. This finding suggests that other sequence and/or conformational features apart from the VAA sequence motif determine the proteolytic degradation of an ASD. While adaptor proteins are known to increase the proteolytic efficiency of ClpX–ClpP proteases in *E. coli* and *B. subtilis* (47), we could not identify a homologous adaptor protein in *M. tuberculosis*. These results suggest that σ^D is activated by the specific proteolysis of the anti-σ factor RsdA, while σ^L is activated by the release of Zn^{2+} from RslA on oxidative stress. In a related finding, *M. tuberculosis* RslA was shown to be a substrate for Rip1, a restricted intramembrane protease. *M. tuberculosis* RsdA, on the other hand, is resistant to proteolysis by *M. tuberculosis* Rip1 (15). This suggests multiple proteolytic cascades dictate the release of specific σ factors. Multiple mechanisms for the release of a σ factor from a σ/anti-σ complex provide an additional strategy to address specific environmental niches. Thus while in one case, the anti-σ factor is proteolytically cleaved by Clp proteases (in the case of RsdA), in the other ASD (RslA) the anti-σ factor is released from its cognate σ factor due to conformational rearrangements on signal recognition (Figure 5).

Put together, the ASD demonstrates surprisingly diverse regulatory mechanisms embedded in a simple four-helical structural scaffold. While structural conservation is essential for binding a cognate σ factor, incorporation of different, perhaps multiple, regulatory mechanisms in an ASD provides a route to achieve temporal changes in σ-factor levels corresponding to diverse environmental stimuli.

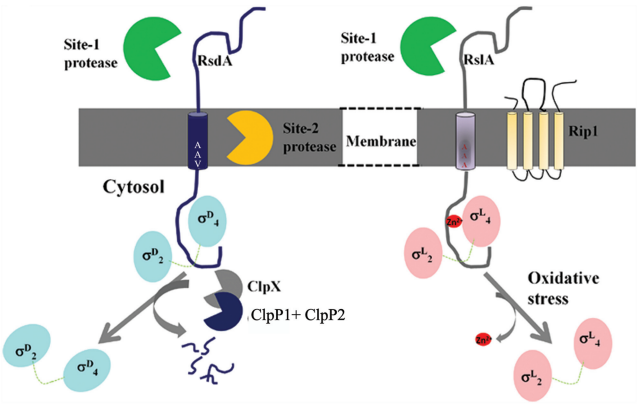

Figure 5. *M. tuberculosis* RsdA and RslA are structurally similar but adopt different regulatory mechanisms. A schematic representation of the mechanisms that govern the release of σ^D and σ^L from their cognate anti-σ factors. σ^D is activated by the proteolytic degradation of RsdA (orange) by ClpX–ClpP1–ClpP2 (sea-green and blue), whereas σ^L is activated on conformational changes in RslA caused by the removal of the Zn^{2+} cofactor. The site-1 and site-2 proteases depicted in this model are putative and based on the characterized *E. coli* model. Both proteases that act on RsdA are yet to be identified in *M. tuberculosis*. The cognate site-2 protease that acts on RslA is Rip1 (15).

ACCESSION NUMBERS

3VFZ, 3VEP.

SUPPLEMENTARY DATA

Supplementary Data are available at NAR Online: Supplementary Tables 1–3, Supplementary Figures 1–5.

ACKNOWLEDGEMENTS

The authors acknowledge the contribution of Dr Krishan Gopal Thakur in the initial stages of this project. The authors gratefully acknowledge Prof. Robert T. Sauer for the Clp knockout strains of *E. coli* that were crucial for this work.

FUNDING

Wellcome Trust, United Kingdom [WT078994MA]; Department of Biotechnology, Government of India. Funding for open access charge: Department of Biotechnology-National Bioscience Award for Career Development (2010–2013).

Conflict of interest statement. None declared.

REFERENCES

1. Rodrigue,S., Provvedi,R., Jacques,P.E., Gaudreau,L. and Manganelli,R. (2006) The sigma factors of Mycobacterium tuberculosis. *FEMS Microbiol. Rev.*, **30**, 926–941.
2. Sachdeva,P., Misra,R., Tyagi,A.K. and Singh,Y. (2009) The sigma factors of Mycobacterium tuberculosis: regulation of the regulators. *FEBS J.*, **277**, 605–626.
3. Baker,T.A. and Sauer,R.T. (2011) ClpXP, an ATP-powered unfolding and protein-degradation machine. *Biochim. Biophys. Acta*, **1823**, 15–28.
4. Hanson,P.I. and Whiteheart,S.W. (2005) AAA+ proteins: have engine, will work. *Nat. Rev. Mol. Cell. Biol.*, **6**, 519–529.
5. Wojtkowiak,D., Georgopoulos,C. and Zylicz,M. (1993) Isolation and characterization of ClpX, a new ATP-dependent specificity component of the Clp protease of Escherichia coli. *J. Biol. Chem.*, **268**, 22609–22617.
6. Wang,J., Hartling,J.A. and Flanagan,J.M. (1997) The structure of ClpP at 2.3 A resolution suggests a model for ATP-dependent proteolysis. *Cell*, **91**, 447–456.
7. Kessel,M., Maurizi,M.R., Kim,B., Kocsis,E., Trus,B.L., Singh,S.K. and Steven,A.C. (1995) Homology in structural organization between E. coli ClpAP protease and the eukaryotic 26 S proteasome. *J. Mol. Biol.*, **250**, 587–594.
8. Chaba,R., Grigorova,I.L., Flynn,J.M., Baker,T.A. and Gross,C.A. (2007) Design principles of the proteolytic cascade governing the sigmaE-mediated envelope stress response in *Escherichia coli:* keys

to graded, buffered, and rapid signal transduction. *Genes Dev.*, **21**, 124–136.
9. Flynn,J.M., Neher,S.B., Kim,Y.I., Sauer,R.T. and Baker,T.A. (2003) Proteomic discovery of cellular substrates of the ClpXP protease reveals five classes of ClpX-recognition signals. *Mol. Cell*, **11**, 671–683.
10. Heinrich,J. and Wiegert,T. (2009) Regulated intramembrane proteolysis in the control of extracytoplasmic function sigma factors. *Res. Microbiol.*, **160**, 696–703.
11. Qiu,D., Eisinger,V.M., Head,N.E., Pier,G.B. and Yu,H.D. (2008) ClpXP proteases positively regulate alginate overexpression and mucoid conversion in *Pseudomonas aeruginosa*. *Microbiology*, **154**, 2119–2130.
12. Zellmeier,S., Schumann,W. and Wiegert,T. (2006) Involvement of Clp protease activity in modulating the *Bacillus subtilis* sigmaW stress response. *Mol. Microbiol.*, **61**, 1569–1582.
13. Raju,R.M., Unnikrishnan,M., Rubin,D.H., Krishnamoorthy,V., Kandror,O., Akopian,T.N., Goldberg,A.L. and Rubin,E.J. (2012) *Mycobacterium tuberculosis* ClpP1 and ClpP2 function together in protein degradation and are required for viability in vitro and during infection. *PLoS Pathog.*, **8**, e1002511.
14. Akopian,T., Kandror,O., Raju,R.M., Unnikrishnan,M., Rubin,E.J. and Goldberg,A.L. (2012) The active ClpP protease from *M. tuberculosis* is a complex composed of a heptameric ClpP1 and a ClpP2 ring. *EMBO J.*, **31**, 1529–1541.
15. Sklar,J.G., Makinoshima,H., Schneider,J.S. and Glickman,M.S. (2010) *M. tuberculosis* intramembrane protease Rip1 controls transcription through three anti-sigma factor substrates. *Mol. Microbiol.*, **77**, 605–617.
16. Thakur,K.G., Praveena,T. and Gopal,B. (2010) Structural and biochemical bases for the redox sensitivity of *Mycobacterium tuberculosis* RslA. *J. Mol. Biol.*, **397**, 1199–1208.
17. Calamita,H., Ko,C., Tyagi,S., Yoshimatsu,T., Morrison,N.E. and Bishai,W.R. (2005) The *Mycobacterium tuberculosis* SigD sigma factor controls the expression of ribosome-associated gene products in stationary phase and is required for full virulence. *Cell. Microbiol.*, **7**, 233–244.
18. Raman,S., Hazra,R., Dascher,C.C. and Husson,R.N. (2004) Transcription regulation by the *Mycobacterium tuberculosis* alternative sigma factor SigD and its role in virulence. *J. Bacteriol.*, **186**, 6605–6616.
19. Shenoy,A.R. and Visweswariah,S.S. (2003) Site-directed mutagenesis using a single mutagenic oligonucleotide and DpnI digestion of template DNA. *Anal. Biochem.*, **319**, 335–336.
20. Battye,T.G., Kontogiannis,L., Johnson,O., Powell,H.R. and Leslie,A.G. (2011) iMOSFLM: a new graphical interface for diffraction-image processing with MOSFLM. *Acta Crystallogr. D Biol. Crystallogr.*, **67**, 271–281.
21. Winn,M.D., Ballard,C.C., Cowtan,K.D., Dodson,E.J., Emsley,P., Evans,P.R., Keegan,R.M., Krissinel,E.B., Leslie,A.G., McCoy,A. *et al.* (2011) Overview of the CCP4 suite and current developments. *Acta Crystallogr. D Biol. Crystallogr.*, **67**, 235–242.
22. Adams,P.D., Afonine,P.V., Bunkoczi,G., Chen,V.B., Davis,I.W., Echols,N., Headd,J.J., Hung,L.W., Kapral,G.J., Grosse-Kunstleve,R.W. *et al.* (2010) PHENIX: a comprehensive Python-based system for macromolecular structure solution. *Acta Crystallogr. D Biol. Crystallogr.*, **66**, 213–221.
23. Emsley,P. and Cowtan,K. (2004) Coot: model-building tools for molecular graphics. *Acta Crystallogr. D Biol. Crystallogr.*, **60**, 2126–2132.
24. Painter,J. and Merritt,E.A. (2006) Optimal description of a protein structure in terms of multiple groups undergoing TLS motion. *J. Appl. Cryst.*, **39**, 109–111.
25. Jorgensen,W., Maxwell,D. and Tirado-Rives,J. (1996) Development and testing of the OPLS all-atom force field on conformational energetics and properties of organic liquids. *J. Am. Chem. Soc.*, **118**, 11225–11236.
26. Van Der Spoel,D., Lindahl,E., Hess,B., Groenhof,G., Mark,A.E. and Berendsen,H.J. (2005) GROMACS: fast, flexible, and free. *J. Comput. Chem.*, **26**, 1701–1718.
27. Berk Hess,H.B., Berendsen,H.J.C. and Fraaije,J.G. (1997) LINCS: a linear constraint solver for molecular simulations. *J. Comput. Chem.*, **18**, 1463–1472.
28. Kabsch,W. and Sander,C. (1983) Dictionary of protein secondary structure: pattern recognition of hydrogen-bonded and geometrical features. *Biopolymers*, **22**, 2577–2637.
29. Smoot,M.E., Ono,K., Ruscheinski,J., Wang,P.L. and Ideker,T. (2011) Cytoscape 2.8: new features for data integration and network visualization. *Bioinformatics*, **27**, 431–432.
30. Thakur,K.G., Jaiswal,R.K., Shukla,J.K., Praveena,T. and Gopal,B. (2010) Over-expression and purification strategies for recombinant multi-protein oligomers: a case study of *Mycobacterium tuberculosis* sigma/anti-sigma factor protein complexes. *Protein Expr Purif*, **74**, 223–230.
31. Campbell,E.A., Greenwell,R., Anthony,J.R., Wang,S., Lim,L., Das,K., Sofia,H.J., Donohue,T.J. and Darst,S.A. (2007) A conserved structural module regulates transcriptional responses to diverse stress signals in bacteria. *Mol. Cell*, **27**, 793–805.
32. Campbell,E.A., Tupy,J.L., Gruber,T.M., Wang,S., Sharp,M.M., Gross,C.A. and Darst,S.A. (2003) Crystal structure of *Escherichia coli* sigmaE with the cytoplasmic domain of its anti-sigma RseA. *Mol. Cell*, **11**, 1067–1078.
33. Lambert,L.J., Wei,Y., Schirf,V., Demeler,B. and Werner,M.H. (2004) T4 AsiA blocks DNA recognition by remodeling sigma70 region 4. *EMBO J.*, **23**, 2952–2962.
34. Vassylyev,D.G., Sekine,S., Laptenko,O., Lee,J., Vassylyeva,M.N., Borukhov,S. and Yokoyama,S. (2002) Crystal structure of a bacterial RNA polymerase holoenzyme at 2.6 A resolution. *Nature*, **417**, 712–719.
35. Lane,W.J. and Darst,S.A. (2006) The structural basis for promoter -35 element recognition by the group IV sigma factors. *PLoS Biol.*, **4**, e269.
36. Patikoglou,G.A., Westblade,L.F., Campbell,E.A., Lamour,V., Lane,W.J. and Darst,S.A. (2007) Crystal structure of the *Escherichia coli* regulator of sigma70, Rsd, in complex with sigma70 domain 4. *J. Mol. Biol.*, **372**, 649–659.
37. Buchan,D.W., Ward,S.M., Lobley,A.E., Nugent,T.C., Bryson,K. and Jones,D.T. (2010) Protein annotation and modelling servers at University College London. *Nucleic Acids Res.*, **38**, W563–W568.
38. Larkin,M.A., Blackshields,G., Brown,N.P., Chenna,R., McGettigan,P.A., McWilliam,H., Valentin,F., Wallace,I.M., Wilm,A., Lopez,R. *et al.* (2007) Clustal W and Clustal X version 2.0. *Bioinformatics*, **23**, 2947–2948.
39. Sharma,A., Sekar,K. and Vijayan,M. (2009) Structure, dynamics, and interactions of jacalin. Insights from molecular dynamics simulations examined in conjunction with results of X-ray studies. *Proteins*, **77**, 760–777.
40. Luo,P. and Baldwin,R.L. (1997) Mechanism of helix induction by trifluoroethanol: a framework for extrapolating the helix-forming properties of peptides from trifluoroethanol/water mixtures back to water. *Biochemistry*, **36**, 8413–8421.
41. Flynn,J.M., Levchenko,I., Sauer,R.T. and Baker,T.A. (2004) Modulating substrate choice: the SspB adaptor delivers a regulator of the extracytoplasmic-stress response to the AAA+ protease ClpXP for degradation. *Genes Dev.*, **18**, 2292–2301.
42. Kim,J.H., Wei,J.R., Wallach,J.B., Robbins,R.S., Rubin,E.J. and Schnappinger,D. (2010) Protein inactivation in mycobacteria by controlled proteolysis and its application to deplete the beta subunit of RNA polymerase. *Nucleic Acids Res.*, **39**, 2210–2220.
43. Barik,S., Sureka,K., Mukherjee,P., Basu,J. and Kundu,M. (2010) RseA, the SigE specific anti-sigma factor of *Mycobacterium tuberculosis*, is inactivated by phosphorylation-dependent ClpC1P2 proteolysis. *Mol. Microbiol.*, **75**, 592–606.
44. Ingvarsson,H., Mate,M.J., Hogbom,M., Portnoi,D., Benaroudj,N., Alzari,P.M., Ortiz-Lombardia,M. and Unge,T. (2007) Insights into the inter-ring plasticity of caseinolytic proteases from the X-ray structure of *Mycobacterium tuberculosis* ClpP1. *Acta Crystallogr. D Biol. Crystallogr.*, **63**, 249–259.
45. Benaroudj,N., Raynal,B., Miot,M. and Ortiz-Lombardia,M. (2011) Assembly and proteolytic processing of mycobacterial ClpP1 and ClpP2. *BMC Biochem.*, **12**, 61.
46. Kim,Y.I., Burton,R.E., Burton,B.M., Sauer,R.T. and Baker,T.A. (2000) Dynamics of substrate denaturation and translocation by the ClpXP degradation machine. *Mol. Cell*, **5**, 639–648.
47. Kirstein,J., Moliere,N., Dougan,D.A. and Turgay,K. (2009) Adapting the machine: adaptor proteins for Hsp100/Clp and AAA+ proteases. *Nat. Rev. Microbiol.*, **7**, 589–599.